in the spinal motor neurons was significantly stronger in the AR-97Q mice at both the before-onset and advanced stages (**Fig. 1d** and **Supplementary Fig. 1a,b**). Although we also detected Cgrp1 in the spinal dorsal horn, the expression of Cgrp1 was not different among the AR-97Q, AR-24Q and wild-type mice (data not shown). Cgrp1 is also expressed in other regions of the central nervous system, although the expression levels in these tissues are much lower than in the spinal cord (**Supplementary Fig. 2a**). Besides the spinal motor neurons, hypoglossal motor neurons and cerebellar granular cells also had high expression of Cgrp1, which accumulated in the cytoplasm of neurons with nuclear accumulation of the pathogenic AR (**Supplementary Fig. 2b,c**). Moreover, immunohistochemical analysis of autopsied human specimens showed higher expression of CGRP1 in the spinal motor neurons of subjects with SBMA compared to controls (**Fig. 1e** and **Supplementary Fig. 3a,b**). Because surgical or pharmacological suppression of testosterone release ameliorates the symptomatic and neuropathological changes in male AR-97Q mice[11,25], we examined the effects of the male sex hormone on the expression of CGRP1 in the mice. Surgical castration significantly decreased the immunoreactivity of Cgrp1 in the male AR-97Q mice (**Fig. 1f**), which is consistent with prior reports demonstrating the expression of CGRP1 is negatively regulated by testosterone[26]. The mRNA levels of *Calca* also decreased as a result of the castration (**Fig. 1g**).

CGRP1 mediates polyglutamine-dependent cytotoxicity

We further investigated the role of CGRP1 in polyglutamine-mediated neurotoxicity in differentiated human neuroblastoma SH-SY5Y cells stably expressing human AR containing 24 or 97 glutamines (AR-24Q and AR-97Q). In this cellular model, polyglutamine-expanded AR induced neurotoxicity and cell death in a testosterone-dependent manner (**Supplementary Fig. 4a–f**). In agreement with the data from the mouse model, cells expressing AR-97Q that were treated with dihydrotestosterone (DHT) had higher levels of *CALCA* mRNA than those bearing AR-24Q (**Fig. 2a**). SH-SY5Y cells expressing the pathogenic AR had higher protein amounts of CGRP1 and luciferase activity under control of the *CALCA* promoter (**Fig. 2b,c**).

We next investigated the relationship between expression of CGRP1 and viability of neuronal cells. Transient overexpression of CGRP1 in SH-SY5Y cells reduced viability and increased cellular damage as measured by the lactate dehydrogenase (LDH) assay (**Fig. 2d,e**). In contrast, siRNA-mediated knockdown of *CALCA* expression diminished the damage and death of cells stably expressing AR-97Q that were treated with DHT (**Fig. 2f,g**). CGRP1 is secreted from neurons, binds its receptors on the cell surface and functions as an autocrine and paracrine factor[27]. We thus examined the effect of CGRP1 on cellular viability via stimulation of its receptor. Administration of synthetic CGRP1 peptides dose-dependently decreased the viability of SH-SY5Y cells (**Fig. 2h**). In contrast, treatment with CGRP8-37, which is an antagonist of the CGRP receptor, attenuated the cytotoxicity caused by the pathogenic AR (**Fig. 2i**).

To confirm the result obtained in SH-SY5Y cell line, we examined the levels of Cgrp1 in mouse primary motor neurons infected with lentiviral vectors containing an N-terminal fragment of human AR with 24 or 97 glutamines (AR-24Q and AR-97Q)[17]. The pathogenic AR formed aggregates (**Supplementary Fig. 5a**) and increased the

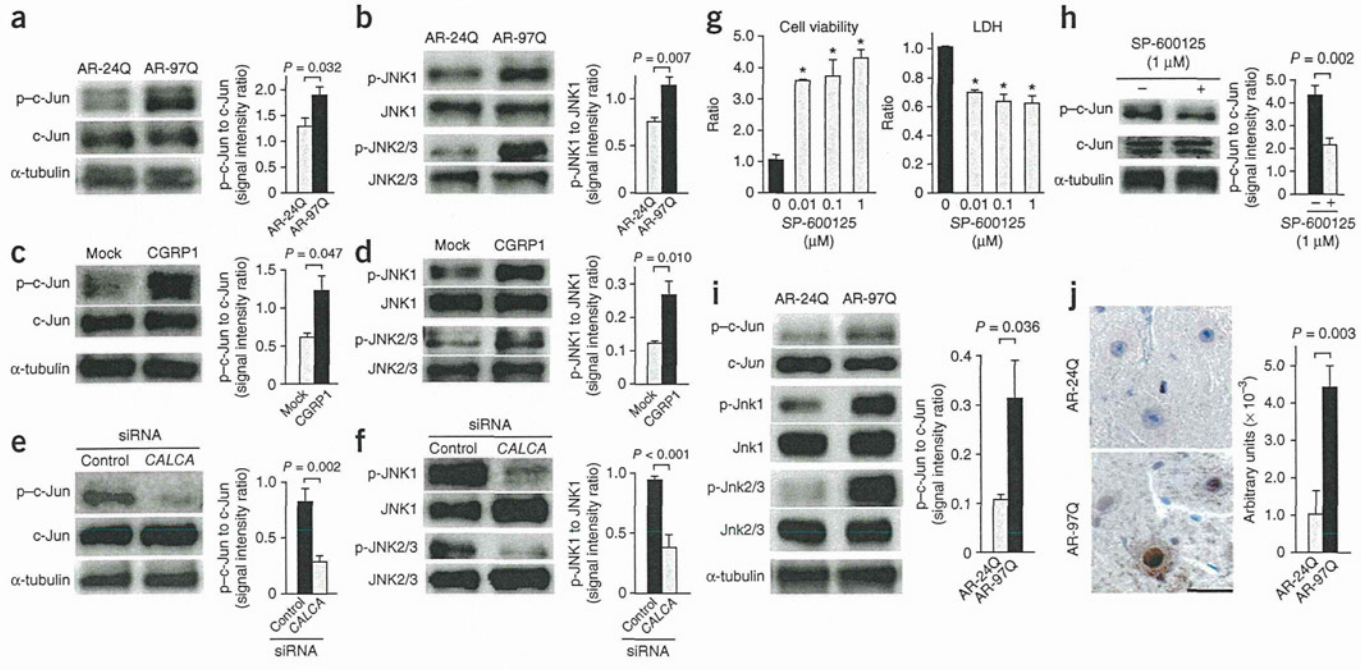

Figure 3 CGRP1 induces neuronal cell damage via activation of the JNK pathway. (**a**,**b**) Immunoblots for c-Jun (**a**) and JNK (**b**) and the relative intensities of immunoreactive bands from SH-SY5Y cells stably expressing AR-24Q and AR-97Q ($n = 6$ per group). (**c**,**d**) Immunoblots for c-Jun (**c**) and JNK (**d**) and the relative intensities of immunoreactive bands from SH-SY5Y cells transfected with the mock or CGRP1 vector ($n = 6$ per group). (**e**,**f**) Immunoblots for c-Jun (**e**) and JNK (**f**) and the relative intensities of immunoreactive bands from SH-SY5Y cells stably expressing AR-97Q transfected with control and *CALCA* siRNA ($n = 6$ per group). (**g**) The viability of (left) and LDH release from (right) SH-SY5Y cells stably expressing AR-97Q treated with a JNK inhibitor, SP-600125 ($n = 6$ per group). (**h**) Immunoblots and relative intensities of p–c-Jun immunoreactive bands from SH-SY5Y cells stably expressing AR-97Q and treated with SP-600125 ($n = 6$ per group). (**i**) Immunoblots (left) and the relative signal intensities (right) of the p–c-Jun immunoreactive bands for spinal cords from the AR-24Q and AR-97Q mice ($n = 6$ per group). (**j**) p–c-Jun immunohistochemistry (left) and the intensity of immunoreactivity to p–c-Jun (right) in spinal motor neurons of AR-24Q and AR-97Q mice ($n = 6$ per group). The scale bar indicates 20 μm. The error bars indicate the s.e.m. $^*P < 0.01$ by ANOVA with Dunnett's test (**g**).

mRNA levels of *Calca* in motor neurons (**Supplementary Fig. 5b**). Furthermore, administration of CGRP1 peptides decreased the viability of primary motor neurons (**Supplementary Fig. 5c**).

CGRP1 induces toxicity via the activation of c-Jun

CGRP1 is known to regulate various cellular signaling pathways, such as nuclear factor-κB (NF-κB) and JNK[28]. We next investigated the molecular mechanism by which CGRP1 elicited neuronal damage (**Supplementary Note** and **Supplementary Fig. 6a–c**). We found that AR-97Q increases the phosphorylation of c-Jun and JNK in neuronal cells treated with DHT (**Fig. 3a,b** and **Supplementary Figs. 7** and **8a**). We also observed activation of the JNK pathway by pathogenic AR in primary motor neurons (**Supplementary Fig. 8b**). Overexpression of CGRP1 also enhanced activation of the JNK pathway in SH-SY5Y cells (**Fig. 3c,d** and **Supplementary Fig. 7b,f**).

To determine whether pathogenic AR stimulates the JNK pathway via the upregulation of CGRP1, we knocked down expression of *CALCA* using siRNA in SH-SY5Y cells stably expressing AR-97Q that are treated with DHT. Transfection of *CALCA* siRNA suppressed activation of the JNK pathway (**Fig. 3e,f** and **Supplementary Fig. 7c,g**). Furthermore, pharmacological inhibition of JNK by SP-600125 increased cell viability and suppressed cytotoxic damage in SH-SY5Y cells stably expressing AR-97Q (**Fig. 3g,h**) and in those treated with CGRP1 peptides (**Supplementary Fig. 8c**). Immunoblot and histopathological analyses also demonstrated activation of the JNK pathway in the AR-97Q mice (**Fig. 3i,j** and **Supplementary Fig. 7d**).

Calca depletion ameliorates motor neuron degeneration

To clarify the role of CGRP1 in the pathogenic processes of SBMA, we next investigated the biological effects of depletion of *Calca* in male AR-97Q mice. Homozygous deletion of the *Calca* gene improved motor function, as assessed by the rotarod task and grip strength, increased body weight and extended the lifespan of the AR-97Q *Calca*$^{-/-}$ mice (**Fig. 4a**). We confirmed that the Cgrp1 protein was depleted in the spinal motor neurons of male AR-97Q *Calca*$^{-/-}$ mice (**Fig. 4b,c**). Histopathological analyses of the skeletal muscles showed that neurogenic amyotrophy was attenuated by depletion of *Calca* (**Fig. 4d**).

Depletion of *Calca* mitigated reactive astrogliosis in the spinal cord of AR-97Q mice, as assessed by GFAP staining at the advanced stage (**Fig. 4e**). Depletion of *Calca* also upregulated the expression of choline acetyltransferase (ChAT), a marker of motor neuronal function (**Fig. 4f,g**). We confirmed that *Calca* depletion had no detectable effects on motor function or ChAT expression in wild-type mice (**Supplementary Fig. 9a–h**). In addition, histopathological and immunoblot analyses showed that deletion of the *Calca* gene suppressed the phosphorylation of c-Jun in the spinal motor neurons of male AR-97Q mice (**Fig. 4h** and **Supplementary Fig. 9i**).

CGRP1 suppression mitigates polyglutamine toxicity

CGRP1 has been implicated in the molecular pathogenesis of migraines, and 5-HT1B/1D receptor agonists have been shown to suppress the expression and secretion of CGRP1 in neurons[29]. We thus determined whether these antimigraine drugs could alleviate polyglutamine-mediated neurotoxicity by decreasing the expression of CGRP1 in neuronal cells. The 5-HT1B/1D receptor agonists sumatriptan, naratriptan and rizatriptan reduced the cellular damage and restored the viability of SH-SY5Y cells that stably expressed AR-97Q (**Fig. 5a**). Given that naratriptan has the longest half-life among these drugs, it may be an appropriate candidate for the treatment

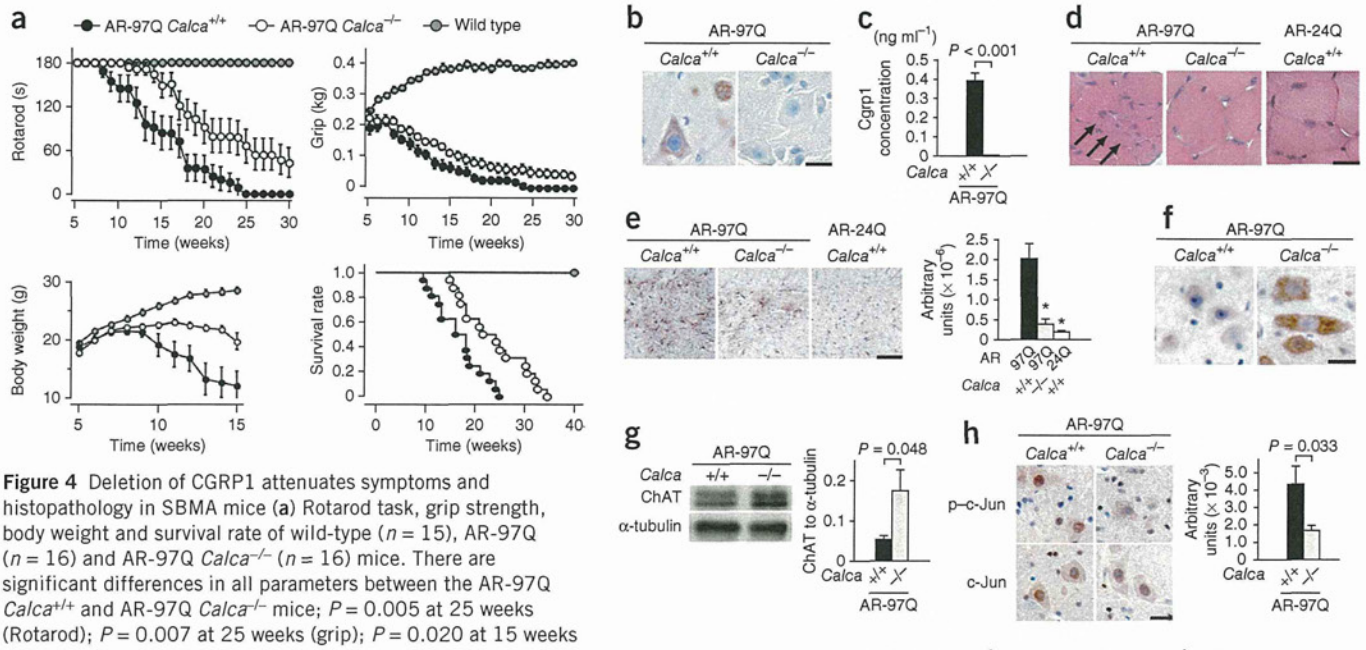

Figure 4 Deletion of CGRP1 attenuates symptoms and histopathology in SBMA mice (**a**) Rotarod task, grip strength, body weight and survival rate of wild-type ($n = 15$), AR-97Q ($n = 16$) and AR-97Q *Calca*$^{-/-}$ ($n = 16$) mice. There are significant differences in all parameters between the AR-97Q *Calca*$^{+/+}$ and AR-97Q *Calca*$^{-/-}$ mice; $P = 0.005$ at 25 weeks (Rotarod); $P = 0.007$ at 25 weeks (grip); $P = 0.020$ at 15 weeks (body weight); and $P = 0.003$ (survival). (**b**) Cgrp1 immunohistochemistry of spinal cords from AR-97Q *Calca*$^{+/+}$ and AR-97Q *Calca*$^{-/-}$ mice (15 weeks old). (**c**) The concentrations of Cgrp1 protein in the spinal cord of AR-97Q *Calca*$^{+/+}$ and AR-97Q *Calca*$^{-/-}$ mice as measured by ELISA ($n = 3$ per group). (**d**) H&E staining of skeletal muscle from AR-97Q *Calca*$^{+/+}$, AR-97Q *Calca*$^{-/-}$ and AR-24Q mice. (**e**) Gfap immunohistochemistry (left) and intensity of immunoreactivity to Gfap (right) in spinal cord sections from AR-97Q *Calca*$^{+/+}$, AR-97Q *Calca*$^{-/-}$ and AR-24Q mice ($n = 6$ per group). (**f**) ChAT immunohistochemistry in spinal cord sections from AR-97Q *Calca*$^{+/+}$ and AR-97Q *Calca*$^{-/-}$ mice. (**g**) Immunoblots (left) and relative signal intensities of ChAT-immunoreactive bands (right) of spinal cords from the AR-97Q *Calca*$^{+/+}$ and AR-97Q *Calca*$^{-/-}$ mice ($n = 6$ per group). (**h**) c-Jun immunohistochemistry (left) and intensity of immunoreactivity to p–c-Jun (right) in spinal cords from AR-97Q *Calca*$^{+/+}$ and AR-97Q *Calca*$^{-/-}$ mice ($n = 6$ per group). The scale bars indicate 20 μm (**b**,**f**,**h**) or 50 μm (**d**,**e**). The error bars indicate the s.e.m. *$P < 0.01$ by ANOVA with Dunnett's test (**e**).

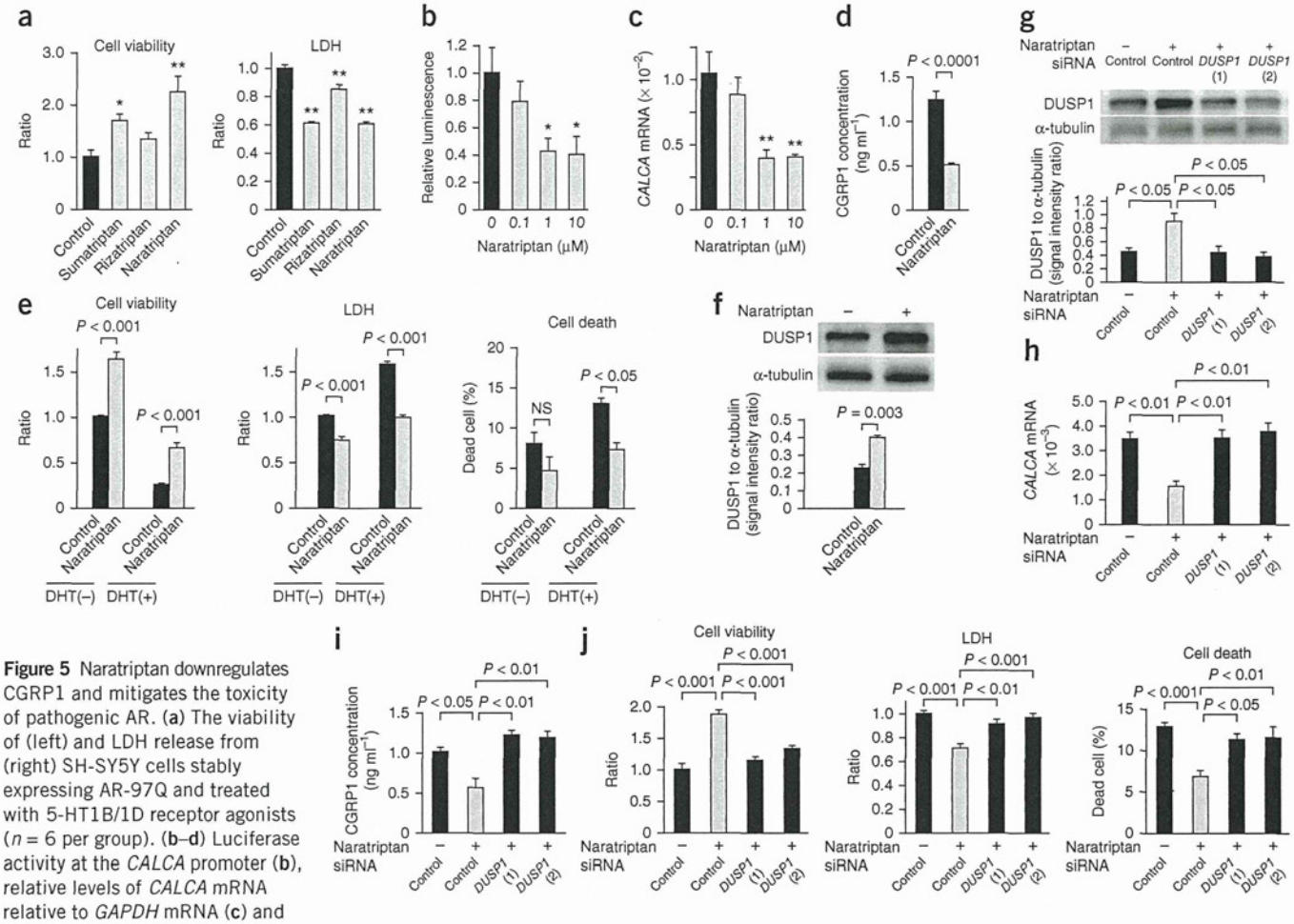

Figure 5 Naratriptan downregulates CGRP1 and mitigates the toxicity of pathogenic AR. (**a**) The viability of (left) and LDH release from (right) SH-SY5Y cells stably expressing AR-97Q and treated with 5-HT1B/1D receptor agonists ($n = 6$ per group). (**b**–**d**) Luciferase activity at the *CALCA* promoter (**b**), relative levels of *CALCA* mRNA relative to *GAPDH* mRNA (**c**) and concentration of CGRP1 (**d**) in SH-SY5Y cells that stably express AR-97Q and were treated with naratriptan ($n = 6$ per group). (**e**) The viability, LDH release and cell death of SH-SY5Y cells stably expressing AR-97Q that were treated with naratriptan and DHT ($n = 6$ per group). (**f**) Immunoblots (top) and relative signal intensities of DUSP1-immunoreactive bands (bottom) of SH-SY5Y cells stably expressing AR-97Q that were treated with or without naratriptan ($n = 3$ per group). (**g**) Immunoblots (top) and relative signal intensities of DUSP1-immunoreactive bands (bottom) of SH-SY5Y cells stably expressing AR-97Q that were transfected with the control or *DUSP1* siRNA and treated with or without naratriptan ($n = 3$ per group). (**h**,**i**) Relative levels of *CALCA* mRNA to *GAPDH* mRNA (**h**) and CRGP1 protein concentration (**i**) in SH-SY5Y cells stably expressing AR-97Q that were transfected with control or *DUSP1* siRNA and treated with naratriptan ($n = 3$ per group). (**j**) Viability, LDH release and cell death of SH-SY5Y cells stably expressing AR-97Q that were transfected with control or *DUSP1* siRNA and treated with naratriptan ($n = 6$ per group). The error bars indicate the s.e.m. $*P < 0.05$ and $**P < 0.01$ by ANOVA with Dunnett's test (**a**–**c**). Statistical analysis was performed using ANOVA with Tukey's test (**g**–**j**). NS, not significant.

of SBMA[30]. Therefore, we investigated the effects of naratriptan on the expression of CGRP1 and on polyglutamine-mediated cytotoxicity in neuronal cells. Administration of naratriptan reduced luciferase activity under control of the *CALCA* promoter as well as the mRNA and protein levels of CGRP1 in SH-SY5Y cells stably expressing AR-97Q (**Fig. 5b–d**). Naratriptan restored cell viability and suppressed the release of LDH, which is a marker of cytotoxicity, in cells treated with or without DHT, although the effects were more pronounced in the presence of DHT (**Fig. 5e**). Moreover, the effects of naratriptan on cell death were observable only when the SH-SY5Y cells expressing AR-97Q were treated with DHT (**Fig. 5e**).

Previous studies have suggested that 5-HT1B/1D receptor agonists suppress the expression of CGRP1 via the induction of DUSP1, a suppressor of the mitogen-activated protein kinase pathway[31]. We thus examined whether the neuroprotective effects of naratriptan are mediated by DUSP1. Naratriptan increased the expression of DUSP1 (**Fig. 5f**). SiRNA-mediated knockdown of *DUSP1* attenuated the effects of naratriptan on CGRP1 expression and neuroprotection in SH-SY5Y cells expressing AR-97Q (**Fig. 5g–j**). Pharmacological inhibition of DUSP1 with Ro-31-8220 in SH-SY5Y cells and primary motor neurons also attenuated naratriptan-mediated neuroprotection (**Supplementary Fig. 10a–g**). Furthermore, pharmacological inhibition of the 5-HT1B/1D receptor also inhibited the effects of naratriptan on CGRP1 expression and neuroprotection (**Supplementary Fig. 11a,b**), confirming that this receptor is involved in naratriptan-mediated suppression of the toxicity of the pathogenic AR.

We next investigated the effects of pharmacological stimulation of the 5-HT1B/1D receptor in a mouse model of SBMA. Oral administration of naratriptan improved grip strength and performance in the rotarod task of male AR-97Q mice in a dose-dependent manner as compared to vehicle-treated control AR-97Q mice (**Fig. 6a**). This pharmacological intervention also increased body weight and lifespan, although it showed no detectable effects on these phenotypes in wild-type mice (**Fig. 6a** and **Supplementary Fig. 12**). In agreement with the results of the cellular experiments, expression

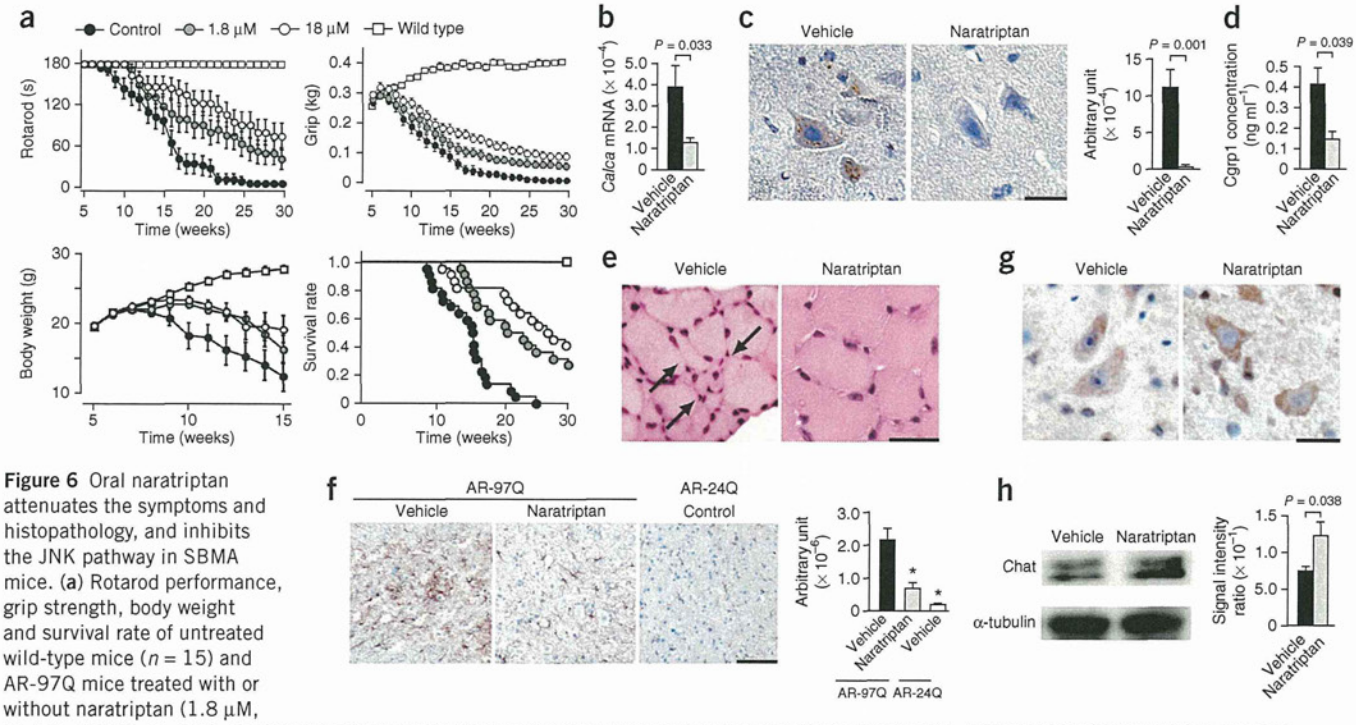

Figure 6 Oral naratriptan attenuates the symptoms and histopathology, and inhibits the JNK pathway in SBMA mice. (**a**) Rotarod performance, grip strength, body weight and survival rate of untreated wild-type mice ($n = 15$) and AR-97Q mice treated with or without naratriptan (1.8 μM, $n = 22$; 18 μM, $n = 22$). Significant differences were observed in all parameters between the untreated ($n = 22$) and 18 μM naratriptan–treated AR-97Q mice: $P < 0.01$ at 25 weeks (rotarod); $P < 0.01$ at 25 weeks (grip); $P < 0.05$ at 15 weeks (body weight); and $P < 0.0001$ (survival). (**b**) Relative levels of *Calca* mRNA to *Gapdh* mRNA in the spinal cords of AR-97Q mice treated with or without naratriptan ($n = 3$ per group). (**c**) Cgrp1 immunohistochemistry and intensity of immunoreactivity to Cgrp1 in spinal cords from AR-97Q mice treated with or without naratriptan ($n = 6$ per group). (**d**) The concentrations of Cgrp1 protein in the spinal cord of AR-97Q mice treated with or without naratriptan ($n = 3$ per group). (**e**) H&E staining of skeletal muscle from AR-97Q mice treated with or without naratriptan. (**f**) Gfap immunohistochemistry (left) and intensity of immunoreactivity to Gfap (right) in spinal cord sections from AR-97Q mice treated with or without naratriptan ($n = 6$ per group). (**g**) ChAT immunohistochemistry in spinal cord sections from AR-97Q mice treated with or without naratriptan. (**h**) Immunoblots and relative intensities of ChAT-immunoreactive bands of spinal cords from AR-97Q mice treated with or without naratriptan ($n = 6$ per group). The scale bars indicate 20 μm (**c**,**g**) or 50 μm (**e**,**f**). The error bars indicate the s.e.m. $^*P < 0.01$ by ANOVA with Dunnett's test (**f**).

of *Calca* was lower in the spinal cords of male AR-97Q mice treated with naratriptan as compared to vehicle-treated controls (**Fig. 6b**). Immunohistochemistry and ELISA revealed that naratriptan suppressed expression of Cgrp1 at the protein level in the spinal motor neurons of SBMA mice (**Fig. 6c,d**). Histopathological analyses indicated that oral naratriptan also reduced muscle wasting, suppressed reactive astrogliosis and increased expression of ChAT in the spinal motor neurons of AR-97Q mice (**Fig. 6e–h**).

Naratriptan suppresses the JNK pathway

To elucidate the molecular basis for the neuroprotection induced by naratriptan, we investigated the effects of this drug on the activity of the JNK pathway. Naratriptan treatment decreased the phosphorylation of c-Jun in SH-SY5Y cells stably expressing AR-97Q and treated with DHT (**Supplementary Fig. 13a,b**). Immunoblotting and immunohistochemistry showed that oral naratriptan also reduced the phosphorylation of c-Jun in the spinal cords of male AR-97Q mice (**Supplementary Fig. 14a,b**). Since the activation of JNK by pathogenic AR disrupts axonal transport, which contributes to the pathogenesis of SBMA[17,32], we investigated the effects of naratriptan on axonal transport. Naratriptan increased the number of motor neurons labeled with FluoroGold, a tracer used to measure retrograde axonal transport in mice (**Supplementary Fig. 15a,b**). As for the safety of naratriptan, we did not observe any adverse effects of oral treatment with naratriptan at 18 μM for 8–10 weeks on liver or renal function (**Supplementary Fig. 15c**).

DISCUSSION

Here we showed that the pathogenic AR protein dysregulates transcription in a mouse model of SBMA before the onset of motor impairment. Among the disease-specific transcriptional changes, CGRP1 was upregulated as the disease progressed and was also found to be upregulated in humans with SBMA and in a cellular model of SBMA. Alterations of gene expression have been demonstrated by microarray analyses of human postmortem specimens and in cellular and animal models of polyglutamine diseases, suggesting that transcriptional dysregulation is central to the pathogenesis of polyglutamine diseases that is independent of the context of the causative protein[22,33,34]. We found that pathogenic AR proteins increase activity at the *CALCA* gene promoter, which indicates that the transcription of CGRP1 is upregulated by pathogenic AR in SBMA.

CGRP1 is known to be upregulated upon neuronal injury, which suggests a potential neuroprotective role of this molecule[35]. On the contrary, elevated expression of CGRP1 is reported to be correlated with increased vulnerability of motor neurons in a mouse model of amyotrophic lateral sclerosis linked to a mutation in the gene encoding superoxide dismutase 1 (SOD1)[36]. Depletion of *Calca*, however, has no effect on the disease progression in mutant *Sod1* mice, suggesting that the basal expression of CGRP1 has neither neurotoxic nor neuroprotective effects[37]. Alternatively, other molecules may overwhelm the effects of CGRP1 on motor neuron degeneration in amyotrophic lateral sclerosis. In contrast, our study shows that increased expression of CGRP1 reduces the viability and induces

damage of neuronal cells. Moreover, genetic suppression of the pathogenic AR–induced upregulation of CGRP1 mitigated neuronal damage in mice. Our findings thus indicate that increased expression of CGRP1 contributes to motor neuron degeneration in SBMA.

CGRP1 is a multifunctional neuropeptide that has a potent vasodilatory effect and is believed to have a key role in vascular headaches[24]. In the nervous system, CGRP1 is also known to regulate nociceptor activation, neuroinflammation and neuronal nicotinic receptor functions[38,39]. Our study shows that overexpression of CGRP1 induces cytotoxicity in neuronal cells, and deletion of *Calca* ameliorates motor neuron damage in the mouse model of SBMA. We also found that pathogenic AR activates the JNK pathway via upregulation of CGRP1 in cellular and mouse models of SBMA. In agreement with our results, CGRP1 was previously shown to activate the JNK pathway in neuroblastoma cells[40]. In addition, we have found that activation of the JNK pathway enhances neuronal damage and that pharmacological inhibition of JNK mitigates the toxicity of pathogenic AR in neuronal cells. Abnormal activation of the JNK pathway has also been implicated in the pathogenesis of neurodegenerative disorders, including SBMA[32,41–44].

On the basis of its potent effects on neuroinflammation, CGRP1 has been identified as a therapeutic target for migraines[45]. Agonists of the 5-HT1B/1D receptor, which are clinically used for the suppression of migraines, reduce the serum levels of CGRP1 (ref. 29). Here we showed that the antimigraine drug naratriptan and other 5-HT1B/1D receptor agonists reduce promoter activity of the gene encoding CGRP1 and decrease mRNA levels of *CALCA* in neuronal cells via the induction of DUSP1. Oral administration of naratriptan also decreased the expression of Cgrp1 and ameliorated the motor impairment in a mouse model of SBMA. Furthermore, our study also showed that naratriptan treatment inhibits the JNK pathway in cellular and mouse models of SBMA. These observations indicate that stimulation of the 5-HT1B/1D receptor suppresses the neurotoxicity of polyglutamine-expanded AR by downregulating CGRP1 resulting in inactivation of the JNK pathway. As naratriptan is widely used in patients with migraine, this drug is a potential candidate for SBMA therapy. However, the efficacy awaits further clinical trials in patients given the limited efficacy of androgen ablation trials, despite the complete suppression of neurodegeneration in AR-97Q mice by leuprorelin[25,46,47]. As naratriptan showed limited effects on survival and motor function in the SBMA model mice, further studies are needed to evaluate the efficacy and safety of long-term treatment with naratriptan in humans.

METHODS

Methods and any associated references are available in the online version of the paper.

Accession codes. Microarray data have been deposited in the Gene Expression Omnibus (GEO) with accession code GSE39865.

Note: Supplementary information is available in the online version of the paper.

ACKNOWLEDGMENTS

This work was supported by a Center-of-Excellence grant, a Grant-in-Aid for Scientific Research on Innovated Areas "Foundation of Synapse and Neurocircuit Pathology" (No. 22110005) and Grants-in-Aid from the Ministry of Education, Culture, Sports, Science and Technology, Japan (Nos. 21229011, 21689024 and 23390230); grants from the Ministry of Health, Labor and Welfare, Japan; Core Research for Evolutional Science and Technology (CREST) from Japan Science and Technology Agency (JST); and a grant from the Kennedy Disease Association.

AUTHOR CONTRIBUTIONS

Project planning was performed by M.M., M.K., H.K. and G.S.; microarray analysis by M.M. and M.K.; cellular analysis by M.M., M.K., H.A., H.D., S.M. and Y.M.; primary motor neuron culture by M.K., S.I. and Y.F.; animal work by M.M., M.K., N.K. and M.I.; tissue staining by M.M., M.K. and M.I.; and data analysis by M.M., M.K., F.T. and G.S. M.M. and M.K. drafted the manuscript, and F.T., H.K. and G.S. revised it critically for intellectual content.

COMPETING FINANCIAL INTERESTS

The authors declare no competing financial interests.

Published online at http://www.nature.com/doifinder/10.1038/nm.2932.
Reprints and permissions information is available online at http://www.nature.com/reprints/index.html.

1. Ross, C.A. & Tabrizi, S.J. Huntington's disease: from molecular pathogenesis to clinical treatment. *Lancet Neurol.* **10**, 83–98 (2011).
2. Gatchel, J.R. & Zoghbi, H.Y. Diseases of unstable repeat expansion: mechanisms and common principles. *Nat. Rev. Genet.* **6**, 743–755 (2005).
3. Finsterer, J. Perspectives of Kennedy's disease. *J. Neurol. Sci.* **298**, 1–10 (2010).
4. Katsuno, M. *et al.* Pathogenesis, animal models and therapeutics in spinal and bulbar muscular atrophy (SBMA). *Exp. Neurol.* **200**, 8–18 (2006).
5. La Spada, A.R., Wilson, E.M., Lubahn, D.B., Harding, A.E. & Fischbeck, K.H. Androgen receptor gene mutations in X-linked spinal and bulbar muscular atrophy. *Nature* **352**, 77–79 (1991).
6. Schmidt, B.J., Greenberg, C.R., Allingham-Hawkins, D.J. & Spriggs, E.L. Expression of X-linked bulbospinal muscular atrophy (Kennedy disease) in two homozygous women. *Neurology* **59**, 770–772 (2002).
7. Sobue, G. *et al.* X-linked recessive bulbospinal neuronopathy. A clinicopathological study. *Brain* **112**, 209–232 (1989).
8. Adachi, H. *et al.* Widespread nuclear and cytoplasmic accumulation of mutant androgen receptor in SBMA patients. *Brain* **128**, 659–670 (2005).
9. Bauer, P.O. & Nukina, N. The pathogenic mechanisms of polyglutamine diseases and current therapeutic strategies. *J. Neurochem.* **110**, 1737–1765 (2009).
10. Shao, J. & Diamond, M.I. Polyglutamine diseases: emerging concepts in pathogenesis and therapy. *Hum. Mol. Genet.* **16 Spec No. 2**, R115–R123 (2007).
11. Katsuno, M. *et al.* Testosterone reduction prevents phenotypic expression in a transgenic mouse model of spinal and bulbar muscular atrophy. *Neuron* **35**, 843–854 (2002).
12. Takeyama, K. *et al.* Androgen-dependent neurodegeneration by polyglutamine-expanded human androgen receptor in *Drosophila*. *Neuron* **35**, 855–864 (2002).
13. Nedelsky, N.B. *et al.* Native functions of the androgen receptor are essential to pathogenesis in a *Drosophila* model of spinobulbar muscular atrophy. *Neuron* **67**, 936–952 (2010).
14. Minamiyama, M. *et al.* Sodium butyrate ameliorates phenotypic expression in a transgenic mouse model of spinal and bulbar muscular atrophy. *Hum. Mol. Genet.* **13**, 1183–1192 (2004).
15. Katsuno, M. *et al.* Reversible disruption of dynactin 1–mediated retrograde axonal transport in polyglutamine-induced motor neuron degeneration. *J. Neurosci.* **26**, 12106–12117 (2006).
16. Ranganathan, S. *et al.* Mitochondrial abnormalities in spinal and bulbar muscular atrophy. *Hum. Mol. Genet.* **18**, 27–42 (2009).
17. Katsuno, M. *et al.* Disrupted transforming growth factor-β signaling in spinal and bulbar muscular atrophy. *J. Neurosci.* **30**, 5702–5712 (2010).
18. Steffan, J.S. *et al.* Histone deacetylase inhibitors arrest polyglutamine-dependent neurodegeneration in *Drosophila*. *Nature* **413**, 739–743 (2001).
19. Butler, R. & Bates, G.P. Histone deacetylase inhibitors as therapeutics for polyglutamine disorders. *Nat. Rev. Neurosci.* **7**, 784–796 (2006).
20. Luthi-Carter, R. *et al.* Decreased expression of striatal signaling genes in a mouse model of Huntington's disease. *Hum. Mol. Genet.* **9**, 1259–1271 (2000).
21. Obrietan, K. & Hoyt, K.R. CRE-mediated transcription is increased in Huntington's disease transgenic mice. *J. Neurosci.* **24**, 791–796 (2004).
22. Sugars, K.L. & Rubinsztein, D.C. Transcriptional abnormalities in Huntington disease. *Trends Genet.* **19**, 233–238 (2003).
23. Mo, K. *et al.* Microarray analysis of gene expression by skeletal muscle of three mouse models of Kennedy disease/spinal bulbar muscular atrophy. *PLoS ONE* **5**, e12922 (2010).
24. Ho, T.W., Edvinsson, L. & Goadsby, P.J. CGRP and its receptors provide new insights into migraine pathophysiology. *Nat. Rev. Neurol.* **6**, 573–582 (2010).
25. Katsuno, M. *et al.* Leuprorelin rescues polyglutamine-dependent phenotypes in a transgenic mouse model of spinal and bulbar muscular atrophy. *Nat. Med.* **9**, 768–773 (2003).
26. Popper, P. & Micevych, P.E. The effect of castration on calcitonin gene–related peptide in spinal motor neurons. *Neuroendocrinology* **50**, 338–343 (1989).
27. Ma, W. *et al.* Localization and modulation of calcitonin gene-related peptide-receptor component protein-immunoreactive cells in the rat central and peripheral nervous systems. *Neuroscience* **120**, 677–694 (2003).
28. Walker, C.S., Conner, A.C., Poyner, D.R. & Hay, D.L. Regulation of signal transduction by calcitonin gene–related peptide receptors. *Trends Pharmacol. Sci.* **31**, 476–483 (2010).

29. Durham, P.L. & Russo, A.F. New insights into the molecular actions of serotonergic antimigraine drugs. *Pharmacol. Ther.* **94**, 77–92 (2002).
30. Jhee, S.S., Shiovitz, T., Crawford, A.W. & Cutler, N.R. Pharmacokinetics and pharmacodynamics of the triptan antimigraine agents: a comparative review. *Clin. Pharmacokinet.* **40**, 189–205 (2001).
31. Durham, P.L. & Russo, A.F. Serotonergic repression of mitogen-activated protein kinase control of the calcitonin gene–related peptide enhancer. *Mol. Endocrinol.* **12**, 1002–1009 (1998).
32. Morfini, G. *et al.* JNK mediates pathogenic effects of polyglutamine-expanded androgen receptor on fast axonal transport. *Nat. Neurosci.* **9**, 907–916 (2006).
33. Serra, H.G. *et al.* Gene profiling links SCA1 pathophysiology to glutamate signaling in Purkinje cells of transgenic mice. *Hum. Mol. Genet.* **13**, 2535–2543 (2004).
34. Becanovic, K. *et al.* Transcriptional changes in Huntington disease identified using genome-wide expression profiling and cross-platform analysis. *Hum. Mol. Genet.* **19**, 1438–1452 (2010).
35. Zheng, L.F. *et al.* Calcitonin gene–related peptide dynamics in rat dorsal root ganglia and spinal cord following different sciatic nerve injuries. *Brain Res.* **1187**, 20–32 (2008).
36. Ringer, C., Weihe, E. & Schutz, B. Calcitonin gene–related peptide expression levels predict motor neuron vulnerability in the superoxide dismutase 1–G93A mouse model of amyotrophic lateral sclerosis. *Neurobiol. Dis.* **45**, 547–554 (2012).
37. Ringer, C., Weihe, E. & Schutz, B. Pre-symptomatic alterations in subcellular betaCGRP distribution in motor neurons precede astrogliosis in ALS mice. *Neurobiol. Dis.* **35**, 286–295 (2009).
38. Di Angelantonio, S., Giniatullin, R., Costa, V., Sokolova, E. & Nistri, A. Modulation of neuronal nicotinic receptor function by the neuropeptides CGRP and substance P on autonomic nerve cells. *Br. J. Pharmacol.* **139**, 1061–1073 (2003).
39. Benemei, S., Nicoletti, P., Capone, J.A. & Geppetti, P. Pain pharmacology in migraine: focus on CGRP and CGRP receptors. *Neurol. Sci.* **28** (suppl. 2), S89–S93 (2007).
40. Disa, J., Parameswaran, N., Nambi, P. & Aiyar, N. Involvement of cAMP-dependent protein kinase and pertussis toxin–sensitive G-proteins in CGRP mediated JNK activation in human neuroblastoma cell line. *Neuropeptides* **34**, 229–233 (2000).
41. Borsello, T. & Forloni, G. JNK signalling: a possible target to prevent neurodegeneration. *Curr. Pharm. Des.* **13**, 1875–1886 (2007).
42. Perrin, V. *et al.* Implication of the JNK pathway in a rat model of Huntington's disease. *Exp. Neurol.* **215**, 191–200 (2009).
43. Mehan, S., Meena, H., Sharma, D. & Sankhla, R. JNK: a stress-activated protein kinase therapeutic strategies and involvement in Alzheimer's and various neurodegenerative abnormalities. *J. Mol. Neurosci.* **43**, 376–390 (2011).
44. Young, J.E. *et al.* Polyglutamine-expanded androgen receptor truncation fragments activate a Bax-dependent apoptotic cascade mediated by DP5/Hrk. *J. Neurosci.* **29**, 1987–1997 (2009).
45. Edvinsson, L. & Goadsby, P.J. Neuropeptides in migraine and cluster headache. *Cephalalgia* **14**, 320–327 (1994).
46. Katsuno, M. *et al.* for the Japan SBMA Interventional Trial for TAP-144-SR (JASMITT) study group. Efficacy and safety of leuprorelin in patients with spinal and bulbar muscular atrophy (JASMITT study): a multicentre, randomised, double-blind, placebo-controlled trial. *Lancet Neurol.* **9**, 875–884 (2010).
47. Fernández-Rhodes, L.E. *et al.* Efficacy and safety of dutasteride in patients with spinal and bulbar muscular atrophy: a randomised placebo-controlled trial. *Lancet Neurol.* **10**, 140–147 (2011).

ONLINE METHODS

Generation, maintenance and treatment of transgenic mice. We generated AR-24Q and AR-97Q male mice as previously described[11,48]. We used AR-97Q (Line #7-8) male mice because they show progressive muscular atrophy and weakness as well as SBMA-like pathology[25,49]. In the appropriate experiments, we administered naratriptan hydrochloride in drinking water (CAS No. 143388-64-1, Toronto Research Chemicals) to mice at a concentration of 1.8 or 18 μM in distilled water from 5 weeks of age until the end of the analysis, as described previously[14]. We performed castration or sham operations on male AR-97Q mice at the age of 5 weeks, as described previously[11,17]. We generated *Calca*-knockout mice (genetic background: 129/Sv × C57BL/6, backcrossed to C57BL/6) as previously described[50] and crossed them with the AR-97Q mice (genetic background: C57BL/6). We also used the littermates for phenotypic analyses. We used only males in this study. Background strain analyses using 96 genome-wide microsatellite markers (Aoba Genetics) demonstrated that the percentage of C57BL/6 was 99.2 ± 0.7% in the *Calca*-knockout mice used in this study. We performed all the animal experiments in accordance with the US National Institutes of Health Guide for the Care and Use of Laboratory Animals and under the approval of the Nagoya University Animal Experiment Committee.

Microarray analysis of mouse spinal cord. We analyzed alterations in gene expression using a GeneChip Mouse Genome 430 2.0 Array (Affymetrix) in male AR-97Q mice because they show a progressive motor dysfunction, muscle weakness and wasting, and they show histopathological evidence of the abnormal accumulation of the pathogenic AR within the nucleus of motor neurons, as is seen in patients with SBMA[22]. For each group (wild-type, AR-24Q and AR-97Q), we examined the male mice at 7–9, 10–12 and 13–15 weeks of age. We chose these stages because the AR-97Q mice are generally asymptomatic at 7–9 weeks of age (before-onset stage), present with mild motor impairment at 10–12 weeks (early stage) and are severely weakened with profound muscle atrophy at 13–15 weeks (advanced stage). RNA from the total spinal cord, excluding the dorsal root ganglia, was isolated from three mice of each genotype at each stage using Trizol reagent (Invitrogen) according to the manufacturer's specifications. The RNA samples were purified over RNeasy columns (Qiagen). TAKARA BIO performed the cDNA preparation, hybridization process and microarray data analysis (GEO accession GSE39865). The probe sets were extracted by the present detection call. We normalized the signals by the trimmed mean method and identified significantly different probe sets ($P < 0.005$) among the strains of mice and stages with a two-way repeated ANOVA. The criterion used to detect the differences in gene expression was a 1.5-fold change.

Assessment of motor ability. We assessed rotarod performance weekly using an Economex Rotarod (Ugo Basile) as described previously[51]. To measure grip strength, the same examiner (M.M.) placed the mice on wire netting with a Grip Strength Meter (MK-380M, Muromachikikai) and pulled them. We performed three trials weekly and recorded the best performance of the grasping power for each mouse with the examiner blinded with respect to the genotype and treatments.

Retrograde FluoroGold neurotracer labeling. We anesthetized the mice with pentobarbital and made a small incision in the skin of the left calf to expose the gastrocnemius muscle. We injected a total volume of 4.5 μl of 2.5% FluoroGold solution (Biotium) in PBS into three different parts of the muscle (proximal, middle and distal) using a 10-μl Hamilton syringe. We removed spinal cords 44 h after FluoroGold administration and post-fixed them with 4% paraformaldehyde in phosphate buffer. We counted the total number of FluoroGold-labeled motor neurons in serial 30-μm spinal cord sections with an Axio Imager M1 (Carl Zeiss).

Hematological analyses of the AR-97Q mice. We collected the blood from the mice at the advanced stage (13–15 weeks) during the dissection performed for the immunohistochemistry and immunoblotting. We measured the ALT and creatinine levels in the serum of the treated mice with the Japan Society of Clinical Chemistry standardization method (MDH-UV method) and the enzymatic method of Mitsubishi Chemical Medicine, respectively.

Plasmids, cell culture and transfection. We isolated SH-SY5Y (American Type Culture Collection No. CRL-2266) mRNA with the RNeasy Mini Kit (Qiagen) and reverse transcribed to yield cDNA. We amplified human *CALCA* cDNA from the SH-SY5Y cDNA with the PrimeStar HS DNA polymerase (Takara Bio) and Takara PCR Thermal Cycler Dice (Takara Bio). We used the following primers: 5′-AGAGGTGTCATGGGCTTCCA-3′ and 5′-GTT GGCATTCTGGGGCATGC-3′. We determined the sequence of the amplified cDNA with a CEQ8000 device (Beckman Coulter). We then cloned the human *CALCA* cDNA into pcDNA3.1/V5-His-TOPO (Invitrogen). For the promoter assay, we transfected GoClone and the pGL4 Luciferase Reporter Vector encoding the *CALCA* promoter (SwitchGear Genomics) into SH-SY5Y cells stably expressing human AR-97Q with Lipofectamine 2000 (Invitrogen). We used the Steady-Glo Luciferase Assay System (Promega) for the measurement of expression with POWERSCAN 4 (DS Pharma Biomedical). The *CALCA* promoter genomic coordinates were chr11-: 14950336–14951268. We plated the wild-type SH-SY5Y cells and those stably expressing the human AR-24Q or AR-97Q and maintained them in DMEM/F12 medium containing 10% FBS with penicillin and streptomycin. We transfected the cells in each dish with the CGRP1 or mock vector using OPTI-MEM (Invitrogen) and Lipofectamine 2000 (Invitrogen) and then differentiated them in DMEM/F12 supplemented with 20 μM retinoic acid and 1 nM 5α-dihydrotestosterone. We added FCS (5%) to the medium for the cell viability assay, but no serum was used for the cell toxicity assay because of the properties of the LDH measurement. We transfected the cells with the CGRP1 vector on days 0 and 2 for the cell viability assay and on day 0 for the LDH assay. We performed both evaluations on day 4. We selected the CGRP1-transfected SH-SY5Y cells for immunoblotting by adding 500 μg ml^{-1} of the antibiotic G418 (Sigma-Aldrich) to the medium 2 d after transfection because of the low transfection efficiency of the cells. We used nontransfected SH-SY5Y cells as selection controls. By 2 weeks after the addition of G418, the control SH-SY5Y cells had died, and we extracted the protein from the surviving CGRP1-transfected SH-SY5Y cells. We isolated human truncated AR cDNAs containing 24 or 97 CAGs (1–645 bp and 1–864 bp, respectively) from pCR3.1-full-length AR-24Q or AR-97Q vector[49] and subcloned them into the pLenti6.3/V5-DEST vector (Invitrogen), of which V5 tag was switched with EmGFP isolated from pcDNA6.2/C-EmGFP-DEST vector (Invitrogen). We transfected 293FT cells (Invitrogen) with the lentivirus vectors using the Virapower lentiviral system (Invitrogen).

SiRNA. We transfected the SH-SY5Y cells stably expressing AR-97Q with the siRNA oligonucleotide duplex at a concentration of 10 nM using Lipofectamine RNAiMAX (Invitrogen), according to the manufacturer's instructions. For knockdown of *CALCA*, we used the following oligonucleotide siRNA duplexes (Takara Bio) to transfect the SH-SY5Y AR-97Q stable cell line: against *CALCA*, sense sequence GUAAUCUGAGUACUUGCA UTT, antisense sequence AUGCAAGUACUCAGAUUACTT; control, sense sequence UCUUAAUCGCGUAUAAGGCTT, antisense sequence GCCUUAUACGCGAUUAAGATT. For knock-down of *DUSP1*, we used the following oligonucleotide siRNA duplexes (Stealth RNAi) to transfect the SH-SY5Y AR-97Q stable cell line: against *DUSP1* (1), sense sequence GACA UGCUGGAUGCCUUGGGCAUAA, antisense sequence UUAUGCCCAAG GCAUCCAGCAUGUC; against *DUSP1* (2), sense sequence GCCAUUGAC UUCAUAGACUCCAUCA, antisense sequence UGAUGGAGUCUAUGAA GUCAAUGGC. We used Stealth RNAi negative control duplex (Invitrogen) as the control for *DSUP1* siRNA.

Primary motor neuron culture. We dissected the spinal cord from C57BL/6 mouse embryos at E13. After removing meninges, dorsal root ganglia and the dorsal half of the spinal cord, we dissociated ventral part tissue into a single-cell suspension by Sumilon dissociation solution (Sumitomo Bakelite). We plated the cells at a density of 2×10^5 cells in a 24-well culture plate with Sumilon nerve-culture medium (Sumitomo Bakelite). On day 4, we infected the neurons with 3×10^5 copies μl^{-1} of lentivirus expressing truncated human AR with 24Q or 97Q[17]. After 3 h of infection, we removed the virus medium. We then cultured the neurons for 3 additional days and harvested them on day 7 followed by RNA extraction, cDNA synthesis, protein extraction, viability assay and immunocytochemistry.

Cell viability and toxicity assays. We performed the cell viability and LDH assays using WST-1 (Roche Diagnostics, Mannheim) and the Cytotoxicity Detection Kit PLUS (Roche Diagnostics), according to the manufacturer's instructions. We determined the number of dead cells using a Countess cell counter (Invitrogen) after staining with Trypan blue. We cultured the cells in 24-well plates. After each treatment, we incubated the cells with the WST-1 substrate for 3–4 h and spectrophotometrically assayed them at 440 nm using a plate reader (Powerscan HT, Dainippon Pharmaceutical). For the toxicity assays, we plated the wild-type SH-SY5Y cells and those stably expressing AR-97Q in the same medium used before transfection. The next day, we differentiated the cells in DMEM/F12 with the same supplement used after transfection. We administered the CGRP1 peptide and the CGRP1 antagonist, CGRP-1 8–37 (Peptide Institute), to the wild-type SH-SY5Y cells and those stably expressing AR-97Q in a serum-free medium for 3 d after differentiation. Two hours after treatment, we performed the cell viability assay. We also administered naratriptan hydrochloride (CAS No. 143388-64-1, Toronto Research Chemicals), rizatriptan benzoate (CAS No. 145202-66-0, Toronto Research Chemicals), sumatriptan succinate (CAS No. 103628-48-4, LKT Laboratories), SP-600125 (Merck), DUSP1 inhibitor (1 μM, Ro-31-8220, Calbiochem) and 5-HT inhibitor methiothepin mesylate (1 μM, sc-253005) in serum-free medium 3 d after differentiation. We administered naratriptan and other triptans at a concentration of 10 μM, unless otherwise mentioned. We performed the cell viability and cytotoxicity assays 24 h after drug administration.

Immunohistochemistry. We deeply anesthetized the mice and removed the entire spinal cord and skeletal muscles. We embedded the mouse samples and the autopsy specimens of the human lumbar spinal cord in paraffin[17] and performed immunohistochemistry and H&E staining as described previously[47,52]. We photographed the immunohistochemical sections with an optical microscope (Axio Imager M1, Carl Zeiss AG, Göttingen, Germany). For blocking/competition, we combined antibody (sc-8856, Santa Cruz, 1:50) with a fivefold (by weight) excess of blocking peptide (Peptide Institute). We obtained the autopsy specimens of the lumbar spinal cord from genetically diagnosed subjects with SBMA (52- and 77-year-old males) and from neurologically normal subjects (53- and 75-year-old males). The Ethics Committee of Nagoya University Graduate School of Medicine approved the collection of human tissues and their use in this study, and we obtained the written informed consent from the subjects' next of kin. We prepared 6-μm-thick sections from paraffin-embedded tissues and used the following primary antibodies: CGRP1 (sc-8856, Santa Cruz, 1:50); p-c-Jun (2361, Cell Signaling Technology, 1:100); c-Jun (#9165, Cell Signaling Technology, 1:400); GFAP (#2301-1, Epitomics, 1:250); and choline acetyltransferase (ab68779, Abcam, 1:1,000). Primary antibody binding was probed with a secondary antibody labeled with a polymer as part of the Envision+ system containing horseradish peroxidase (Dako). We measured the immunoreactivity of CGRP1 in the spinal motor neurons of SBMA and control subjects within five nonconsecutive sections with an interval of 30 μm from three subjects of each group. For the purposes of counting, we defined a motor neuron by its presence within the anterior horn and the obvious nucleolus in a given 6-μm-thick section. We calculated the intensities by multiplying the staining concentration by cell sizes using WinROOF (Mitani). We measured the immunoreactivity of p–c-Jun in more than 20 neurons within three nonconsecutive sections from each mouse ($n = 6$). For the purposes of counting, we defined a motor neuron as described above. We quantified the intensities and cell sizes with WinROOF. The means ± s.e.m. were expressed in arbitrary units.

Immunocytochemistry. We fixed mouse primary motor neurons with 4% paraformaldehyde, treated with 5% Triton X-100 and incubated them with the following primary antibodies: neurofilament H (SMI32, Covance, 1:500), GFP (598 or M048-3, MBL, 1:500) and p–c-Jun (2361, Cell Signaling Technology, 1:500).

Immunoblotting. We deeply anesthetized the mice with pentobarbital anesthesia, dissected the tissues (whole brains, spinal cords, brainstems and skeletal muscles), snap-froze them with powdered CO_2 in acetone and homogenized them in PhosphoSafe Extraction Reagent (Merck Chemicals) containing phosphatase inhibitor and HALT, which is a protease inhibitor cocktail (Thermo Scientific). We lysed the cultured cells in the same reagent after intervention. We used NE-PER Nuclear Cytoplasmic Reagents (Thermo Scientific) for the analysis of the NF-κB pathway. We separated the samples on 5–20% SDS-PAGE gels and then transferred them to Hybond-P membranes (GE Healthcare) using 25 mM Tris, 192 mM glycine, 0.1% SDS and 10% methanol as the transfer buffer. We diluted the primary and secondary antibodies with Can Get Signal, which is a signal enhancer solution (NKB-101, Toyobo). We digitized the immunoblots with an LAS-3000 imaging system (Fujifilm), quantified the signal intensities of the independent blots with Image Gauge software, version 4.22 (Fujifilm), and expressed the means ± s.e.m. in arbitrary units. We used the following primary antibodies: p–c-Jun (#2361, Cell Signaling Technology, 1:1,000); c-Jun (ab16777, Abcam, 1:40); p-JNK (NB110-66666, Novus Biologicals, 1:1,000); JNK (#9252, Cell Signaling Technology, 1:1,000); choline acetyltransferase (ab68779, Abcam, 1:1,000); DUSP1 (sc-1199, Santa Cruz, 1:100); p-NFKBIA (#9241, Cell Signaling Technology, 1:1,000); NFKBIA (#1130-1, Epitomics, 1:10,000); NF-κB p65 (sc-8008, Santa Cruz, 1:200); NF-κB p50 (sc-8414, Santa Cruz, 1:200); histone H1 (sc-8030, Santa Cruz, 1:100); α-tubulin (T5168, Sigma-Aldrich, 1:5000); phospho-ERK1/2 (4370, Cell Signaling Technology, 1:2,000); and ERK1/2 (#4695, Cell Signaling Technology, 1:1,000). We probed the primary antibody binding using horseradish peroxidase–conjugated secondary antibodies (GE Healthcare) at a dilution of 1:5,000, and detected the bands using the ECL Plus kit (GE Healthcare).

Quantitative real-time PCR. We determined the mRNA levels of the examined genes by real-time PCR as described previously[15,52]. Briefly, we extracted total RNA from the mouse spinal cords using TRIzol Reagent (Invitrogen) and from the cells using the RNeasy Mini Kit (Qiagen). We then reverse transcribed the extracted RNA into first-strand cDNA using SuperScript III reverse transcriptase (Invitrogen). We performed real-time PCR in a total volume of 50 μl that contained 25 μl 2× QuantiTect SYBR Green PCR Master Mix and 0.4 μM of each primer (Qiagen), and we detected the amplified products by the iCycler system (Bio-Rad Laboratories). The reaction conditions were 95 °C for 15 min, followed by 45 cycles of 15 s at 95 °C, 30 s at 55 °C and 30 s at 72 °C. As an internal control, we simultaneously quantified the expression level of glyceraldehyde-3-phosphate dehydrogenase (*GAPDH*). We used the following primers: 5′-GAAGAAGAAGTTCGCCTGCT-3′ and 5′-GATTCCCACACCGCTTAGAT-3′ for mouse *Calca*, 5′-CCTGGAGAAACCTGCCAAGTAT-3′ and 5′-TGAAGTCGCAGGAGACAACCT-3′ for mouse *Gapdh*, 5′-ACTGGTGCAGGACTATGTGC-3′ and 5′-CTTGTTGAAGTCCTGCGTGT-3′ for human *CALCA*, and 5′-AGCCTCAAGATCATCAGCAAT-3′ and 5′-GGACTGTGGTCATGAGTCCTT-3′ for human *GAPDH*. The weight of the gene contained in each sample was equal to the log of the starting quantity, and the standardized expression level of each mouse was equal to the weight ratio of each gene to that of *Gapdh*. We repeated the PCRs three times for each of the indicated numbers of samples.

ELISA. We extracted the lysates of the SH-SY5Y cells stably expressing AR-24Q and AR-97Q with CelLytic-M (Sigma-Aldrich) after each intervention. We used the CGRP EIA kit (Phoenix Pharmaceuticals), and corrected the loading dose with a PathScan Total α-Tubulin Sandwitch Elisa Kit (Cell Signaling Technology).

Statistical analyses. We analyzed the data using the Kaplan-Meier and log-rank tests for the survival rate, the unpaired *t*-test for two-group comparisons, and ANOVA with Dunnett's or Tukey's *post hoc* tests for multiple comparisons. We performed the statistical analyses using Statview software version 5 (HULINKS) and Prism version 4 (GraphPad Software).

48. Niwa, H., Yamamura, K. & Miyazaki, J. Efficient selection for high-expression transfectants with a novel eukaryotic vector. *Gene* **108**, 193–199 (1991).
49. Waza, M. *et al.* 17-AAG, an Hsp90 inhibitor, ameliorates polyglutamine-mediated motor neuron degeneration. *Nat. Med.* **11**, 1088–1095 (2005).
50. Oh-hashi, Y. *et al.* Elevated sympathetic nervous activity in mice deficient in alphaCGRP. *Circ. Res.* **89**, 983–990 (2001).
51. Adachi, H. *et al.* CHIP overexpression reduces mutant androgen receptor protein and ameliorates phenotypes of the spinal and bulbar muscular atrophy transgenic mouse model. *J. Neurosci.* **27**, 5115–5126 (2007).
52. Tokui, K. *et al.* 17-DMAG ameliorates polyglutamine-mediated motor neuron degeneration through well-preserved proteasome function in an SBMA model mouse. *Hum. Mol. Genet.* **18**, 898–910 (2009).

nature medicine

Viral delivery of miR-196a ameliorates the SBMA phenotype via the silencing of CELF2

Yu Miyazaki[1], Hiroaki Adachi[1], Masahisa Katsuno[1], Makoto Minamiyama[1], Yue-Mei Jiang[1], Zhe Huang[1], Hideki Doi[1], Shinjiro Matsumoto[1], Naohide Kondo[1], Madoka Iida[1], Genki Tohnai[1], Fumiaki Tanaka[1], Shin-ichi Muramatsu[2] & Gen Sobue[1]

Spinal and bulbar muscular atrophy (SBMA) is an inherited neurodegenerative disorder caused by the expansion of the polyglutamine (polyQ) tract of the androgen receptor (AR-polyQ)[1,2]. Characteristics of SBMA include proximal muscular atrophy, weakness, contraction fasciculation and bulbar involvement[3]. MicroRNAs (miRNAs) are a diverse class of highly conserved small RNA molecules that function as crucial regulators of gene expression in animals and plants[4]. Recent functional studies have shown the potent activity of specific miRNAs as disease modifiers both *in vitro* and *in vivo*[5–8]. Thus, potential therapeutic approaches that target the miRNA processing pathway have recently attracted attention[9,10]. Here we describe a novel therapeutic approach using the adeno-associated virus (AAV) vector–mediated delivery of a specific miRNA for SBMA. We found that miR-196a enhanced the decay of the AR mRNA by silencing CUGBP, Elav-like family member 2 (CELF2). CELF2 directly acted on AR mRNA and enhanced the stability of AR mRNA. Furthermore, we found that the early intervention of miR-196a delivered by an AAV vector ameliorated the SBMA phenotypes in a mouse model. Our results establish the proof of principle that disease-specific miRNA delivery could be useful in neurodegenerative diseases.

A mouse model of SBMA has been developed[11], and several therapeutic approaches for SBMA have been presented using this mouse model[11–15]. Among these approaches, the reduction of mutant AR protein levels in male mice ameliorated disease manifestations, suggesting a potential therapy for SBMA. miRNAs guide the RNA-induced silencing complex to mRNAs that have a target sequence complementary to that of the miRNA. The interaction between the miRNA and the target can occur with an incomplete complementary sequence; thus, a single miRNA can modulate complex physiological functions or disease phenotypes by regulating widespread networks[16]. Over the last several years, an important role of miRNAs in the pathogenesis of neurodegenerative disorders has been reported[5–8,17,18].

In this study, we used a miRNA microarray analysis to compare the miRNA expression in the spinal cords of male transgenic SBMA model mice expressing full-length human AR with 97 glutamine residues (AR-97Q) and in male mice expressing wild-type human AR (AR-24Q)[11]. Of more than 500 miRNAs tested, miR-196a (accession number MIMAT_0000518), miR-196b (accession number MIMAT_0001081), miR-496 (accession number MIMAT_0003738), miR miR-323-3p (accession number MIMAT_0000551) and miR-29b* (accession number MIMAT_0004523) showed a greater than two-fold upregulation in the spinal cord of AR-97Q mice at an advanced disease stage relative to the AR-24Q mice (**Fig. 1a**).

To examine the effects of these five miRNAs on the expression levels of AR mRNA transcribed from the *AR* gene, we co-transfected synthetic miRNAs with vectors expressing human AR-24Q or AR-97Q into HEK293T cells. Among these five miRNAs, miR-196a and miR-196b downregulated the AR mRNA and protein (**Fig. 1b,c**), although the transgene used in both the *in vitro* and *in vivo* experiments lacked the DNA sequence that encodes the AR mRNA 3′ untranslated region (UTR) (**Supplementary Fig. 1**). To determine whether the decrease in the AR mRNA level was due to the enhancement of mRNA degradation or a decrease in mRNA synthesis, we assessed the turnover of AR mRNA using an RNA stability assay with actinomycin D. In the absence of miR-196a and miR-196b, the AR mRNA had a half-life of >1.5 h. The AR mRNA had a half-life of <0.5 h in the presence of miR-196a and miR-196b (**Fig. 1d**). These findings indicated that miR-196a and miR-196b enhanced the degradation of AR mRNA via an interaction with cofactors that were able to stabilize both the wild-type and mutant AR mRNAs.

To elucidate the molecular mechanisms by which miR-196a and miR-196b regulate the stability of AR mRNA, we analyzed their potential targets using the bioinformatics program TargetScan Release 6.0. Among the hundreds of mRNAs targeted by miR-196a and miR-196b, CELF2 mRNA has a common binding site for miR-196a and miR-196b that is broadly conserved among vertebrates (**Supplementary Fig. 2**). We found that CELF2 mRNA and protein levels were significantly reduced by treatment with miR-196a and miR-196b in HEK293T cells (**Fig. 1e**) and that CELF2 was required for AR mRNA stability

[1]Department of Neurology, Nagoya University Graduate School of Medicine, Nagoya, Japan. [2]Division of Neurology, Department of Medicine, Jichi Medical University, Tochigi, Japan. Correspondence should be addressed to G.S. (sobueg@med.nagoya-u.ac.jp).

Received 3 October 2011; accepted 18 April 2012; published online 3 June 2012; doi:10.1038/nm.2791

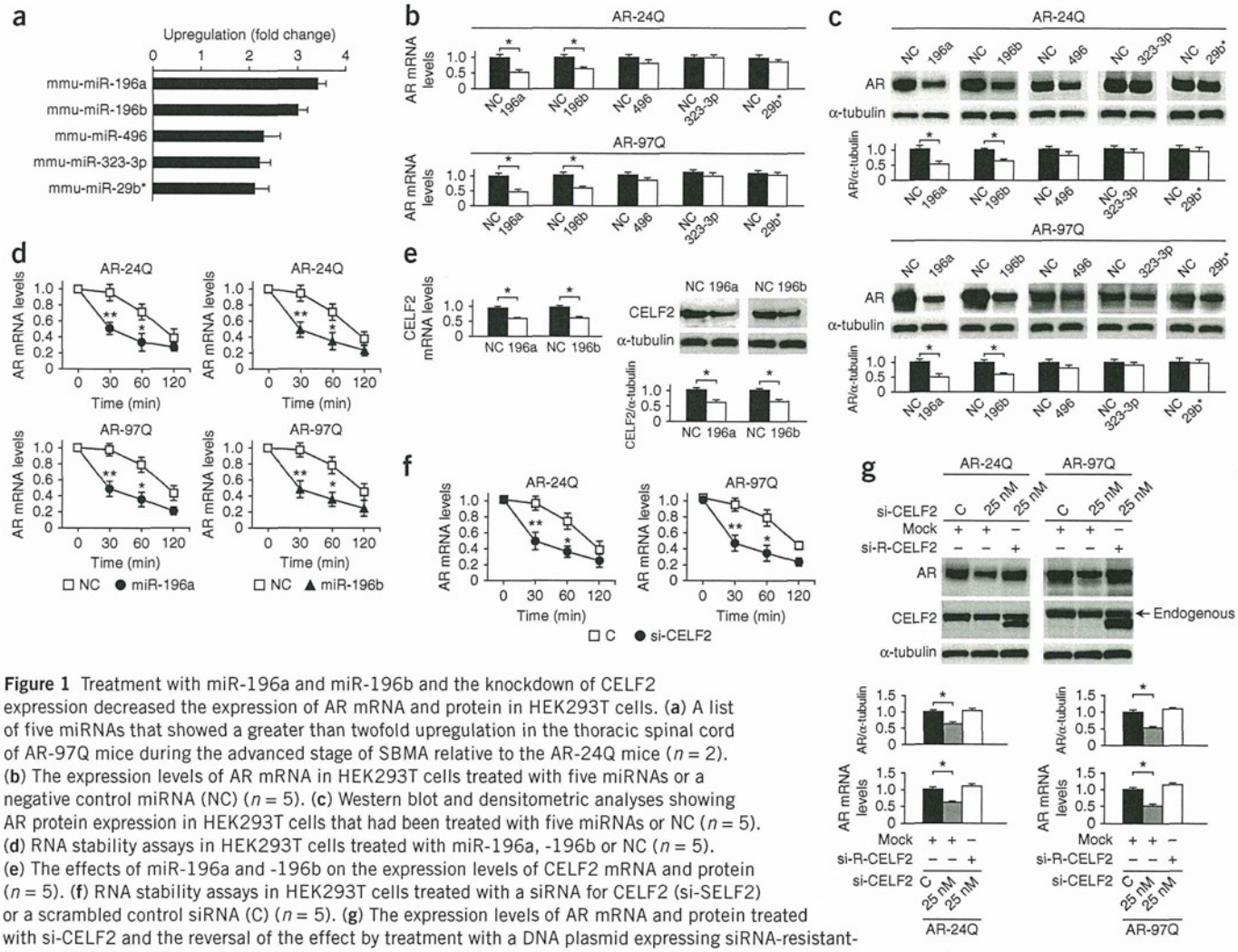

Figure 1 Treatment with miR-196a and miR-196b and the knockdown of CELF2 expression decreased the expression of AR mRNA and protein in HEK293T cells. (**a**) A list of five miRNAs that showed a greater than twofold upregulation in the thoracic spinal cord of AR-97Q mice during the advanced stage of SBMA relative to the AR-24Q mice ($n = 2$). (**b**) The expression levels of AR mRNA in HEK293T cells treated with five miRNAs or a negative control miRNA (NC) ($n = 5$). (**c**) Western blot and densitometric analyses showing AR protein expression in HEK293T cells that had been treated with five miRNAs or NC ($n = 5$). (**d**) RNA stability assays in HEK293T cells treated with miR-196a, -196b or NC ($n = 5$). (**e**) The effects of miR-196a and -196b on the expression levels of CELF2 mRNA and protein ($n = 5$). (**f**) RNA stability assays in HEK293T cells treated with a siRNA for CELF2 (si-SELF2) or a scrambled control siRNA (C) ($n = 5$). (**g**) The expression levels of AR mRNA and protein treated with si-CELF2 and the reversal of the effect by treatment with a DNA plasmid expressing siRNA-resistant-CELF2 (si-R-CELF2) ($n = 5$). All data are means ± s.e.m. $^*P < 0.05$ and $^{**}P < 0.01$. We analyzed the results by unpaired *t* tests in **b**, **c** and **e**; by two-way ANOVA followed by the Bonferroni test comparing HEK293T cells treated with miR-196a or miR-196b to cells treated with NC in **d**; by two-way ANOVA followed by the Bonferroni test comparing HEK293T cells treated with si-CELF2 to cells treated with control siRNA in **f**; and by the Dunnett test in **g**.

(**Fig. 1f**). The knockdown of CELF2 expression with specific small interfering RNAs (siRNAs) silenced CELF2 protein, accelerated the degradation of AR mRNA and led to a decrease in AR protein expression levels (**Fig. 1g**). These downregulating effects were reversed in rescue experiments using a DNA plasmid that expressed siRNA-resistant CELF2, thus confirming the interaction between CELF2 and AR mRNA (**Fig. 1g**). In contrast to the knockdown and rescue results, the overexpression of CELF2 increased the expression levels of AR mRNA and protein (**Fig. 2a**) and increased the stability of the AR mRNA (**Fig. 2b**). To determine the region of the AR mRNA that interacts with CELF2, we prepared several constructs of the mutated *AR* transgene that lacked the CAG repeats (AR-0Q) or the three triplet repeats of the CUGCUGCUG sequence (ΔCUG-AR-24Q and ΔCUG-AR-97Q), which is immediately proximal to the CAG repeats in exon 1 of the AR mRNA and is conserved in the endogenous human AR mRNA (**Fig. 2c**). Although the overexpression of CELF2 increased the expression levels of AR mRNA and protein transcribed from the mutated transgene lacking CAG repeats, the expression levels of AR mRNA and protein transcribed from the mutated transgene lacking the three triplet repeats of the CUGCUGCUG sequence were not increased relative to controls by CELF2 (**Fig. 2d**). In addition, immunoprecipitation-coupled quantitative real time-PCR (qRT-PCR) revealed the binding affinity of CELF2 to the three triplet repeats of the CUGCUGCUG sequence in exon 1 of the AR mRNA (**Fig. 2e**). On the basis of these findings, we concluded that miR-196a and miR-196b were able to decrease the expression levels of AR mRNA and protein by silencing CELF2, a protein that enhances the stability of AR mRNA through direct binding to the CUG triplet repeat sequence in exon 1 of the AR mRNA.

To examine the effects of CELF2 silencing on the motor impairment of SBMA mice, we constructed an *in vivo* delivery system based on an AAV vector that allowed for the simultaneous expression of enhanced green fluorescent protein (EGFP) and either miR-196a (AAV-miR-196a) or a nonspecific miRNA, miR-mock (AAV-miR-mock). We chose to use miR-196a instead of miR-196b because the expression of miR-196a was highly upregulated in the cytoplasm of the motor neurons of AR-97Q mice (**Supplementary Fig. 3**). A viral load of 10^{11} vector genomes (vg) of each of these constructs was injected into the skeletal muscle of the left quadriceps femoris of AR-97Q mice. The AAV vector can be transported efficiently in a retrograde manner from muscle to the motor neurons of the spinal cord[19,20] and can spread hematogenously[21,22]. Two weeks after AAV vector injection,